# Synthesis, Structure, and Physical Properties of Hybrid Nanocomposites for Solid-State Dye Lasers

**I. García-Moreno,* A. Costela, and A. Cuesta**

*Instituto de Química-Física "Rocasolano", C.S.I.C., Serrano 119, 28006 Madrid, Spain*

**O. García, D. del Agua, and R. Sastre**

*Instituto de Ciencia y Tecnología de Polímeros, C.S.I.C., Juan de la Cierva 3, 28006 Madrid, Spain*

*Received: February 25, 2005*

We report on the synthesis, structural characterization, physical properties, and lasing action of two organic dyes, Rhodamine 6G (Rh6G) and Pyrromethene 597 (PM597), incorporated into new hybrid organic−inorganic materials, where the organic component was either poly(2-hydroxyethyl-methacrylate) (PHEMA) or copolymers of HEMA with methyl methacrylate (MMA), and the inorganic counterpart consisted of silica derived from hydrolysis−condensation of methyltriethoxysilane (TRIEOS) in weight proportion of up to 30%. Lasing efficiencies of up 23% and high photostabilities, with no sign of degradation in the initial laser output after 100 000 pump pulses at 10 Hz, were demonstrated when pumping the samples transversely at 534 nm with 5.5 mJ/pulse. A direct relationship could be established between the structure of the hybrid materials, analyzed by solid-state NMR, and their laser behavior. An inorganic network dominated by di-/tri- substituted silicates in a proportion ≈35:65, corresponding to samples of HEMA with 15 and 20 wt % proportion of TRIEOS, optimizes the lasing photostability. The thermal properties of these materials, together with the high homogeneity revealed by atomic force microscopy (AFM) images, even in compounds with high silica content, indicate their microstructure to be a continuous phase, corresponding to the polymer matrix, which "traps" the silica components at molecular level via covalent bonding, with few or no silica islands.

## I. Introduction

The methods of the sol−gel chemistry have represented a real breakthrough in the use of molecular chemistry for the design of new materials. They allow the synthesis of hybrid organic−inorganic compounds which combine the advantages of inorganic glasses (high thermal dissipation capability, low thermal expansion and thermal coefficient of refractive index d$n$/d$T$, and high damage threshold)[1−4] with those offered by organic polymers (high capacity to solve organic dyes, good homogeneity, adaptability to techniques of cheap production, and relative easiness to modify the material's structure and chemical composition).[4−8] The transparency and stability of these new materials make them very suitable for optical and optoelectronics applications in fields of high technical and economical importance such as the development of solid-state dye lasers.

Organic−inorganic hybrid materials have been already tried as solid hosts for lasing dyes.[9−17] Lasing efficiencies of up to 66%, depending on the type of lasing cavity and the pump parameters, and good photostabilities, with an output reduction of less than 15% after 106 000 pump pulses, have been reported with dyes of the rhodamine and pyrromethene families.[12,18] However, further progress in a material's photostability would be necessary before an operational solid-state dye laser was a commercial alternative to conventional liquid solution dye lasers.[19] In fact, for practical applications (i.e., dermatology treatment) a stable output of at least 300 000 pump pulses would be needed. In addition, an important problem manifested in these hybrid materials is an optical homogeneity not good enough for applications requiring high beam quality.[13, 20,21]

To design hybrid matrixes doped with organic dyes with improved laser performance, it would be of great value to study, in a systematic way, the dependence of the laser action on the chemical structure and physical properties of the final material. Control of the properties of the final material can be achieved by modifying the composition, monomer functionality, chemical nature of the organic and inorganic phases, size, and morphology of these domains, from nanometer (nanocomposites) to subnanometer (molecular composites) scales, as well as the nature of the interphase interactions.[22]

To this aim, in the present work, we have synthesized new hybrid organic−inorganic materials, doped with dyes Rhodamine 6G (Rh6G) and Pyrromethene 597 (PM597), based on poly(2-hydroxyethyl methacrylate) (PHEMA) or 1:1 v/v copolymers of methyl methacrylate (MMA) with HEMA as an organic component with increased weight proportions of methyltriethoxysilane (TRIEOS) as inorganic precursor. This trialkoxide was chosen to decrease the cross-linking density of the inorganic network regarding the one obtained when classic tetrafunctional alkoxides, such as tetraethoxysilane or tetramethoxysilane, are used. In addition, the presence in the structure of the TRIEOS of a methyl group remainder after its hydrolysis process would favor the compatibility between the inorganic and organic phases in the final hybrid material.

The laser action of both Rh6G and PM597 chromophores was studied under transversal pumping at 532 nm with nanosecond pulses of 5.5 mJ and at a repetition rate of 10 Hz. The organization of the molecular units in these nanostructured

* Corresponding author. E-mail: iqrfm84@iqfr.csic.es.

10.1021/jp058076a CCC: $30.25 
Published on Web 10/29/2005

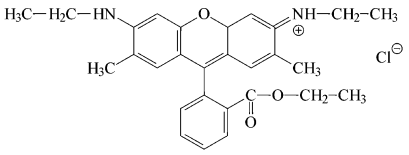

**(Rh6G)**

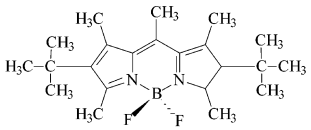

**(PM 597)**

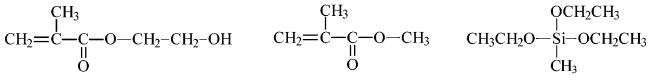

2-hydroxyethyl methacrylate **(HEMA)**

methyl methacrylate **(MMA)**

methyl triethoxysilane **(TRIEOS)**

**Figure 1.** Molecular structure of Rh6G and PM597 dyes, organic monomers HEMA and MMA, and inorganic alkoxide TRIEOS.

solid materials was studied through a structural analysis by solid-state NMR. The composition, stability, and thermal properties of the final material were analyzed by Fourier transform infrared spectroscopy (FT-IR), thermogravimetry (TGA), and differential scanning calorimetry (DSC). The microscopic morphological features of these hybrid materials related to both their chemical composition and optical properties were examined by atomic force microscopy (AFM).

## II. Experimental Section

**Materials.** Rhodamine 6G as chloride salt and Pyrromethene 597 (laser grade, Lambda Physik) were used as received with a purity >99% (checked by spectroscopic and chromatographic methods). 2-Hydroxyethyl methacrylate (HEMA) and methyl methacrylate (MMA) were purchased from Aldrich. Both monomers were freshly distilled and dried under reduced pressure before use. Methyltriethoxysilane (TRIEOS) (ABCR, purity of 99%) and hydrochloric acid (35%) (HCl) from Panreac were used as received without further purification. Pyridine, used as a neutralization agent, was distilled under reduced pressure and kept dry over molecular sieves of 4 Å. 2,2′-Azobis-(isobutyronitrile) (AIBN), used as polymerization initiator, was purchased from Aldrich, was recrystallized in ethanol before use. The molecular structures of dyes, alkoxide, and monomer molecules selected in this work are shown in Figure 1.

**Synthesis.** The synthesis route of these hybrid materials is based on the "in situ" and simultaneous hydrolysis−condensation of the inorganic TRIEOS during the free radical polymerization of the organic monomers. The copolymer MMA/HEMA 1:1 was chosen for PM597 by taking into account the good laser performance previously obtained with this dye in organic matrixes with this composition, while pure HEMA is required for the total solubility of Rh6G.

Because of the presence of OH side groups in HEMA, no addition of solvents was necessary because this monomer acts as a good cosolvent of the selected trialkoxide, allowing the maintenance of a viscosity low enough to achieve a good mixing level. In addition, the hydroxyl groups can participate in the polycondensation process of the alkoxide, improving the organic−inorganic compatibility and allowing an interpenetrated polymer−silica morphology with excellent optical transparency to be obtained.

The sol−gel process of the alkoxide was catalyzed by adding, under continuous stirring, a mixture of water and hydrochloric acid (HCl), maintaining in all cases the following molar ratios: [HCl]/[TRIEOS] = $1.85 \times 10^{-2}$ and [$H_2O$]/[TRIEOS] = 1.5. The total content of the silica precursors has been adjusted as a function of the maximum proportion content in silicon that allowed the synthesis of hybrid monoliths under proper conditions, that is without suffering break and maintaining good optical properties. In the present case, this content was varied from 5% until a maximum of 30% weight proportion in the final hybrid material was reached.

The theoretical prediction of the total content of silica present in the hybrid has been calculated assuming that the sol−gel reactions are complete:

$$CH_3Si(O\text{-}C_nH_{2n}+1)_3 + H_2O \rightarrow CH_3SiO_3 + 3C_nH_{2n+1} - OH$$

In these cases, the following equation has been applied:

$$\frac{m_2}{m_1} = \left(\frac{1}{\alpha} - 1\right)\frac{M_{SiO_2}}{M_{TRIEOS}}$$

where $m_1$ and $m_2$ are the masses of alkoxide and acrylic monomer, respectively; $\alpha$ is the silica content of the resulting hybrid; and $M_{SiO_2}$ (≈60 g/mol) and $M_{TRIEOS}$ (≈178 g/mol) are the molecular weights of silica and the alkoxide, respectively.

The adequate amount of laser dye was dissolved in the corresponding organic monomer mixture to achieve a final concentration of $4 \times 10^{-4}$ M and $6 \times 10^{-4}$ M for Rh6G and PM597, respectively, and the resulting solutions were placed in an ultrasonic bath to ensure the complete dissolution of the dye. The simultaneous organic polymerization was carried out by radical bulk polymerization by using the thermal initiator AIBN in an appropriate concentration (0.5 wt %) with regard to the total amount of monomers in the polymerization mixture. AIBN is the thermal polymerization initiator of choice because it leaves UV-transparent end groups on the so-obtained copolymer. Because we found that pyrromethene dyes lose their lasing ability under acid or basic conditions,[14] pyridine was added to the TRIEOS solution in order to decrease the acidity up to pH > 6, before the addition of the monomer mixture that included PM597 as dye, which was dropped under stirring to the initial hydrolyzed TRIEOS solution.

As an example of the preparing procedure, the detailed steps followed in the preparation of HEMA/TRIEOS 10 wt % (this percentage is related to the total content of silica present in the hybrid, calculated assuming that the sol−gel reactions are complete) doped with Rh6G were as next described:

First, if a final volume of 6 mL is required, 26 $\mu$L of hydrochloric acid solution (35%) and 0.13 mL of water are added to 0.0083 mol of TRIEOS (1.66 mL), under continuous stirring, during 30 min. On the other hand, 0.035 mol of HEMA (4.2 mL), 0.022 g of AIBN (0.5 wt %), and the dye (Rh6G, $4 \times 10^{-4}$ M) are mixed together and filtered using a 0.45 $\mu$m pore size filter followed by a 0.2 $\mu$m pore size filter (Whatman Lab., poly(tetrafluoroethylene) disposable filters). The final organic solutions were then dropped under stirring on the TRIEOS solution. The resulting mixture is kept under vigorous stirring for another 30 min. Then, it was poured into cylindrical molds of polypropylene (≈14 mm diameter) with the purpose of obtaining a geometric configuration close to that required by the final solid dye laser sample. The molds were then heated in an oven at 45−50 °C during ≈1−2 months, followed by a slow increasing of temperature, until reaching 80 °C, during one week. Finally, the temperature was reduced in steps of 5

°C per day until room temperature was reached, and only then were the samples unmolded. Hybrid cylindrical solid monoliths of ≈3−4 $cm^3$ were so obtained having good mechanical properties.

**Characterization.** A differential scanning calorimeter (DSC-6, Perkin-Elmer) was used for investigating the glass transition temperature ($T_g$) of the new hybrid materials. DSC scans of the hybrid materials, as very fine powder, were conducted under nitrogen atmosphere at a heating rate of 20 °C/min, from 20 °C to 150 °C.

Thermogravimetric analysis (TGA) of the hybrid materials, as very fine powder, were performed on a thermogravimetric analyzer (TGA 7, Perkin-Elmer) under nitrogen atmosphere at a heating rate of 10 °C/min, from 20 °C to 800 °C.

Infrared spectra of the samples, as powder-pressed KBr pellets, were recorded on a Fourier transform infrared spectrophotometer (spectrum RX I FT-IR system, Perkin-Elmer) in the spectral range of 4000−400 $cm^{-1}$.

Refractive index of the solid hybrid samples were measured at room temperature by using an Abbe refractometer (model D-7082, Carl Zeiss) employing 1-bromonaphthalene as sample-support interphase and a sodium lamp as monochromatic light at 589 nm.

$^{13}C$ and $^{29}Si$ NMR experiments were performed in a Bruker Avance 400 spectrometer (Bruker Analytik GmbH, Karlsruhe, Germany) equipped with a Bruker UltraShield 9.4-T ($^{13}C$ and $^{29}Si$ resonance frequencies of 100.62 and 79.49 MHz, respectively), 8.9-cm vertical-bore superconducting magnet. In both cases, CP-MAS NMR spectra were acquired at ambient temperature by using a standard Bruker broadband MAS probe. Representative samples were ground and packed in 4 mm zirconia rotors, sealed with Kel-F caps and spun at 5 kHz. The 90° pulse width was 3.5−4.5 $\mu$s, and in all cases, high-power proton decoupling was used. All free induction decays were subjected to standard Fourier transformation and phasing. The chemical shifts were externally referenced to TMS.

The $^{13}C$ CP-MAS NMR spectra were acquired with 1 ms CP contact time and 5 s recycle delay. Each spectrum was obtained with 800 averages and 5 Hz line broadening.

The $^{29}Si$ CP-MAS NMR spectra were obtained with 4 ms CP contact time, 5 s recycle delay, 6.000 averages and 75 Hz line broadening. The spectra were deconvoluted by using Gaussian fits, in terms of $T_i$ where $i = 1, 2, 3$, corresponding to the number of siloxane bridges bonded to the silicon atom of interest. The NMR spectra were evaluated with the software package XWIN NMR provided by Bruker.

Topographical and lateral force atomic force microscopic (AFM) images were recorded simultaneously in the contact mode with a Topometrix TMX 2010 Discoverer scanning probe microscope by using commercial silicon nitride ($Si_3N_4$) probe tips placed at the end of a V-type cantilever. Roughness values, measured from topographic AFM images, are given as the average roughness, $R_A$, defined as:

$$R_A = \frac{1}{N}\sum_{i=1}^{N} |Z_i - \bar{Z}|$$

where $Z_i$ is the height of every pixel in the AFM image and $\bar{Z}$ is the average height, defined as:

$$\bar{Z} = \frac{1}{N}\sum_{i=1}^{N} Z_i$$

**Laser Experiments.** The solid monolith laser samples were cast in a cylindrical shape, forming rods of 10 mm diameter and 10 mm length. A cut was made parallel to the axis of the cylinder to obtain a lateral flat surface of ≈6 × 10 mm. This surface as well as the ends of the laser rods were prepared for lasing experiments by using a grinding and polishing machine (Phoenix Beta 4000, Buehler) until optical-grade finished. The planar grinding stage was carried out with a Texmet 1000 sand paper (Buehler) using a diamond polishing compound of 6 $\mu$m as an abrasive in mineral oil as a lubricant. The final polishing stage was realized with a G-Tuch Microcloth (Buehler), using a cloth disk Mastertex (Buehler) with diamond of 1 $\mu$m in mineral oil as an abrasive type.

The hybrid rods were transversely pumped at 534 nm with 5.5 mJ, 6 ns fwhm pulses from a frequency-doubled Q-switched Nd:KGW laser (Monocrom STR-2+) at a repetition rate of 10 Hz. Same samples were also pumped at 30 Hz with a Nd:YAG laser (Monocrom EO Q-DPSSL 532) under otherwise identical experimental conditions. The exciting pulses were directed toward the lateral flat surface of the sample with a combination of spherical ($f = 50$ cm) and two cylindrical quartz lenses. The first one, with $f = -15$ cm, widened the spherical cross section of the pump beam to illuminate the complete 1 cm length of the dye sample; then, the second lens, with $f = 15$ cm and perpendicularly arranged, focused the pump pulses onto the input surface of the solid sample to form a line of 0.3 × 10 mm so that the pump fluence was 180 mJ/$cm^2$. The oscillator cavity consisted of a ≈90% reflectivity flat aluminum mirror and the end face of the solid sample as the output coupler, with a cavity length of 2 cm.

The dye and pump laser pulses were characterized with the following instruments: GenTec ED-100A and ED-200 pyroelectric energy meters, ITL TF1850 fast rise time photodiode, Tektronix 7934 storage oscilloscope and TDS 3032 digital phosphor oscilloscope, SpectraPro-300i monochromator (Acton Research Corporation), and Hamamatsu R928 photomultiplier. The dye and pump laser signals were sampled with boxcars (Stanford Research Model 250). All the integrated signals were digitized and processed using a PC computer via a Computerboard DASH-8 interface.[23] The estimated error of the energy measurements was about 10%.

## III. Results and Discussion

**Lasing Properties.** Broadband laser emission with a pulse duration of ≈13 ns fwhm and beam divergence of ≈5 mrad was obtained from all the monolith materials under study. Laser emission maxima (Table 1) of Rh6G and PM597 incorporated into these hybrid matrixes were established in the 569−576 nm spectral range, depending on the hybrid composition, with oscillation bandwidths of ≈5 nm, typical of a laser with many modes running simultaneously due to the lack of wavelength-selection elements in the cavity. Increasing the proportion of TRIEOS in the matrix results in red-shifts of the maxima of both the fluorescence and the laser spectra, probably related to changes in the polarity of the media.

The lasing efficiencies of Rh6G and PM597 in the different hybrid formulation under study, defined as the ratio between the energy of the dye laser output and the energy of the pump laser incident on the sample surface, are reported in Table 1. Values up to 23% with PM597 and up to 16% for Rh6G were obtained with no clear dependence on the matrix composition. The lasing efficiency of the dye incorporated into these sol−gel materials could be limited, to some extent, by internal scattering losses due to the refractive index mismatch between

**TABLE 1: Influence of the Increasing Weight Proportion of TRIEOS on the Laser Parameters[a] for Both Rh6G Incorporated in PHEMA and PM597 Doped Copolymers of MMA/HEMA 1:1 v/v Proportion**

| material | Rh6G[b] | | | PM597[b] | | | |
|---|---|---|---|---|---|---|---|
| wt TRIEOS | $\lambda_{max}$ (nm) | eff (%) | $I_n$ (%)[c] | $\lambda_{max}$ (nm) | eff (%) | $I_n$ (%) | $I_n$ (%)[d] |
| 5% | 569 | 16 | 30 | 573 | 19 | 121 | 1 |
| 10% | 571 | 10 | 42 | 575 | 23 | 135 | 18 |
| 15% | 572 | 10 | 180 | 576 | 21 | 123 | 33 |
| 20% | 573 | 10 | 230 | | | | |
| 25% | 573 | 13 | 51 | | | | |
| 30% | 573 | 13 | 35 | | | | |

[a] $\lambda_{max}$: wavelength peak of the laser emission and eff: energy conversion efficiency. [b] [Rh6G] = $4 \times 10^{-4}$ M. [PM597] = $6 \times 10^{-4}$ M. Nd:YAG pump energy: 5.5 mJ/pulse, repetition rate: 10 Hz. [c] Intensity of the dye laser output after $n$= 100 000 pump pulses referred to the initial intensity $I_0$, $I_n$ (%) = $(I_n/I_0) \times 100$. [d] Intensity of the dye laser output after $n$ = 60 000 pump pulses referred to the initial intensity $I_0$, $I_n$ (%) = $(I_n/I_0) \times 100$ at 30 Hz repetition rate, under otherwise identical experimental conditions.

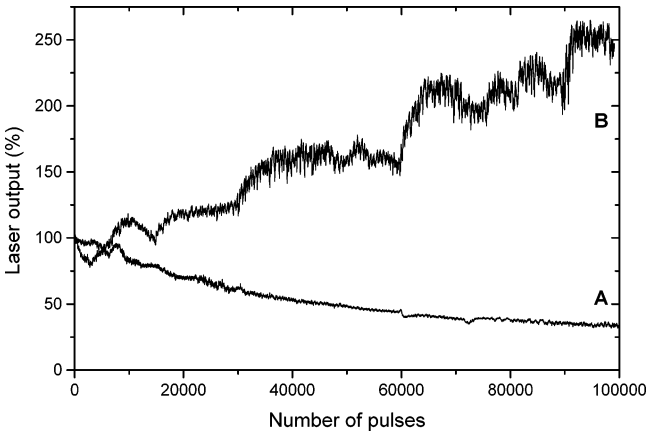


**Figure 2.** Laser output as a function of the number of pump pulses for Rh6G dissolved in PHEMA with different wt % proportions of TRIEOS: (A) = 5% and (B) = 20%. Pump energy and repetition rate: 5.5 mJ/pulse and 10 Hz, respectively. Dye concentration: $4 \times 10^{-4}$ M.

the organic and inorganic phases. As the lasing sample is pumped, waste heat is initially deposited in the organic phase, followed by thermal diffusion into the glass, with the temperature distributions eventually reaching a steady state. Given the different values of d$n$/d$T$ for glass and polymer, the two hybrid components should ideally be index matched for the anticipated thermal loading in order to improve energy efficiencies and spatial properties of the laser action based in these materials.

The evolution of the laser output as a function of the number of pump pulses was studied for the different materials at a repetition rate of 10 Hz. The experimental results are reported in Table 1. Figure 2 shows the photostability of Rh6G embedded in matrixes based on PHEMA with 5 and 20 wt % of TRIEOS. Putting aside for the moment the continuous increase in the laser output energy of Rh6G in the samples with 15% and 20% TRIEOS, it is seen from Table 1 that the lasing photostability of these dye results to be very dependent on the inorganic content of the matrix, with the lasing lifetime initially increasing with the proportion of TRIEOS and peaking at the composition with 20 wt % of this inorganic compound. This effect can be attributed to a slowing down in the diffusion of oxygen as well as to the improvement in the thermal dissipation and resistance of the hybrid material, which reduces the thermal degradation of the dye under laser radiation.[10,11] A higher proportion of the

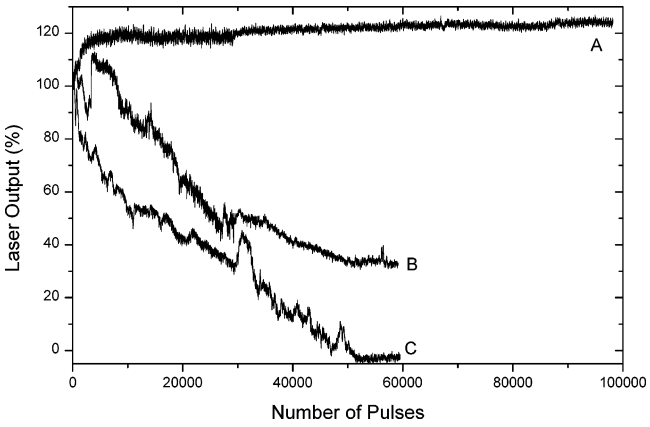


**Figure 3.** Dependence on the pumping repetition rate of the lasing photostability of PM597 doped matrixes of P(MMA/HEMA 1:1) with different wt % proportions of TRIEOS: (A) = 15% and 10 Hz, (B) = 15% and 30 Hz, and (C) = 5% and 30 Hz. Dye concentration: $6 \times 10^{-4}$ M.

alkoxide in the matrix is detrimental to the laser action, with a progressive shortening of the photostability. By taking into account that the dye molecules are confined in the organic part, and this decreases as the inorganic component increases, the observed behavior could be explained as direct consequence of the apparent higher concentration of the dye in the organic part of these hybrid materials. As a result, the photochemical degradation of the dye molecules is enhanced and a fraction of the dye molecules are converted in active species (radicals, triplets), which, in turn, react with nearby dye molecules, impurities, radicals, and labile groups from the polymer chains or other adventitious active species present in the material.

The influence of the inorganic proportion on the lasing photostability of PM597 is reported in Table 1. The photostabilty of PM597 dye exhibits a different behavior to that described above for Rh6G because, over 100 000 pump pulses at a 10 Hz repetition rate, the evolution of the laser output of the dye is independent of the inorganic composition of the samples. It seems that the dissipation channels for the energy released to the medium as heat are able to dissipate the excess energy fast enough in all cases when the repetition rate was 10 Hz, resulting in a stability similar in the three selected matrixes. Thus, we proceeded next to pump the hybrid matrixes doped with PM597 at the more demanding repetition rate of 30 Hz under otherwise identical experimental conditions. In Figure 3, the evolution of the laser output as a function of both the number of pump pulses and the repetition rate is shown graphically for matrixes based on MMA/HEMA 1:1 v/v with 5 and 15 wt % proportion of TRIEOS. As thermal degradation of the dye is enhanced when the pump repetition rate is increased,[14] it is to be expected that under these conditions a dependence of the lasing stability with the matrix composition would be observed.

It can be seen from Table 1 and Figure 3 that increasing the repetition rate to 30 Hz results in changes in the PM597 degradation depending on the inorganic content of the hybrid matrix: the higher the weight proportion of the TRIEOS, the higher the photostability of the dye due to the enhancement of the thermal dissipation provided by the silica phase. In matrixes doped with the dye PM597, the experimental conditions needed to carry out the sol−gel process do not allow an increase of the content of TRIEOS over 15 wt % proportion because increasing the inorganic proportion into the material increases the remanent acidity of the medium, which, for pyrromethene dyes, could boost off reactive processes and, consequently, the degradation of the dye. Work in progress is directed to find out

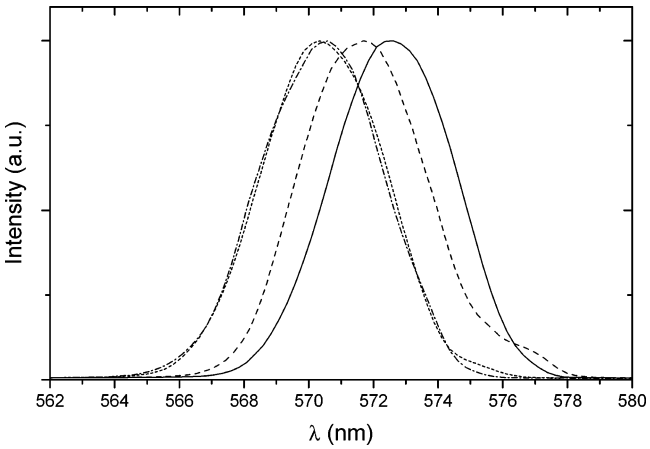


**Figure 4.** Evolution of the laser wavelength for Rh6G incorporated into (PHEMA 15 wt % TRIEOS) matrix as a function of the number of pump pulses: 2 pulses (solid line), 2000 pulses (dashed line), 5000 pulses (dotted line), and 6000 pulses (dashed−dotted line).

new and more efficient neutralization routes thath will allow obtaining of hybrid matrixes with higher weight proportion of silica doped with pyrromethene dyes.

It has to be pointed out that the photostability exhibited by these materials is the highest obtained up to date with Rh6G incorporated into inorganic, organic, and sol−gel hybrid hosts, even when considering samples pumped under soft conditions: longitudinal configuration and at low repetition rates.[9,13] There are not data in the literature on the laser emission of PM597 dye in purely organic matrixes. Lasing efficiencies as high as 60% under 532 nm pumping were obtained when dye PM597, in concentration similar to that used in the present work, was incorporated into hybrid xerogel matrixes, but pumping was longitudinal and the lasing cavity optimized.[24] When pumped with 1.8 mJ/pulse at 10 Hz repetition rate, the laser emission dropped to 75% of its initial value after 100 000 pump pulses.[24]

In all of the reported experiments, the lasing photostability was limited by dye photobleaching and not by optical damage to the matrix. Even with the more demanding transversal pumping conditions utilized in our work, no progressive microfracturing effects related to differences in the thermal expansion coefficients of the two hybrid components were observed.

During the stability experiments, a small blue-shift of $\approx$3 nm in the laser wavelength was observed, which can be understood as being due to a decrease of the dye concentration along the gain length.[16] This wavelength shift essentially ceases after 6000 pump pulses and is identical for all the materials studied. For the sake of clarity, the evolution of the laser wavelength as a function of the number of pump pulses is presented in Figure 4. As indicated above, this behavior could be related to photobleaching of the dye molecules through an oxidation process induced in the surface of the matrix by the pumping radiation. As the more external dye molecules are gradually degraded, a new region of the sample behind the first layer is exposed to subsequent excitation pulses, with the result of the gain region moving through the sample. In fact, after irradiation, a conical-like irradiated volume is observed. It has to be pointed out that the photostability measurements were recorded at the shifted wavelengths.

The above behavior is different from that exhibited for the dye molecules when they are incorporated into pure organic matrixes. In this case, the structure and composition of the material define a static irradiated region so that the same volume of the sample is pumped during all of the experiment, and after irradiation, some irreversible changes in the form of a dark nonemissive line in the region pumped do appear. In the present hybrid matrixes, the absence of dye molecules in the inorganic domains and the homogeneous distribution of these domains into the sample allows for the pump radiation to advance continuously, penetrating deeper into the monolith and increasing in this way the thickness of the irradiated area. Consequently, the photostability measurements are reflecting the dynamics of the replacement of bleached molecules for some nonphotodegraded ones in the extended pumped volume, and the concrete structure and composition of the matrix are the main factors influencing the laser photostability. Thus, while the laser emission from the samples doped with Rh6G and with a 5, 10, 25, and 30 wt % proportion of TRIEOS remains, after 100 000 pump pulses, at 30, 42, 51, and 35%, respectively, of their initial laser output, this parameter increases significantly, by factors 1.7 and 2.5, respectively, for matrixes with 15 and 20 wt % proportion of TRIEOS. In these last two cases, an already low photodegradation rate of active molecules results were compensated by the presence into the gain region of new dye molecules highly stabilized by the structure and composition of the mentioned matrixes. For this reason, the irradiated volume could become, in same way, "overconcentrated" with respect to the beginning of the stability measurements, leading to the observed increase in the laser output.

To gain a better insight into the parameters that optimize the laser action of the dye/hybrid systems, an exhaustive study on structure−property relationships was carried out, analyzing the composition, morphology, and a number of physical properties of these hybrid materials.

**Morphology Study.** The thermal, optical, and laser properties of the hybrid materials depend to a great extent on the compatibility between the organic polymer and the silica component. To investigate the distribution of silica and microphase separation in the hybrid matrix, the morphology of solid samples based on PHEMA with 15 and 30 wt % proportion of TRIEOS were analyzed by AFM. In these studies, the surface of samples grinded and polished to the quality needed for laser experiments was analyzed together with fresh fracture surfaces prepared by breaking the monolithic samples immediately prior to the measurements in order to check the possible influence of the grinding and polishing processes on the morphology of the final samples.

Figure 5 shows the topography and lateral force (friction) images of the samples with 15 and 30 wt % proportion of TRIEOS. Despite the difference in the TRIEOS content, the surfaces of both samples show a very similar topography, characterized by rather flat domains crossed by cracks and scratches, although the roughness of the sample containing 30 wt % TRIEOS, measured from large scale ($>5 \times 5\ \mu m^2$) images, is higher ($R_A = 32.8$ nm) than that of the sample containing only 15% TRIEOS ($R_A = 18.8$ nm). It could be thought that the increase in the proportion of the inorganic content could affect the magnitude of cross-linking between phases and the dispersion of silica particles into the polymeric matrix. Nevertheless, the lateral force images of these samples are also very similar, and they do not show in any case any clear indication of phase segregation between organic and inorganic domains. Although some areas appear slightly brighter than others in the friction images, their close resemblance to the topography image and the fact that most of the features observed coincide with topographic accidents prevent identifying them with segregated domains.

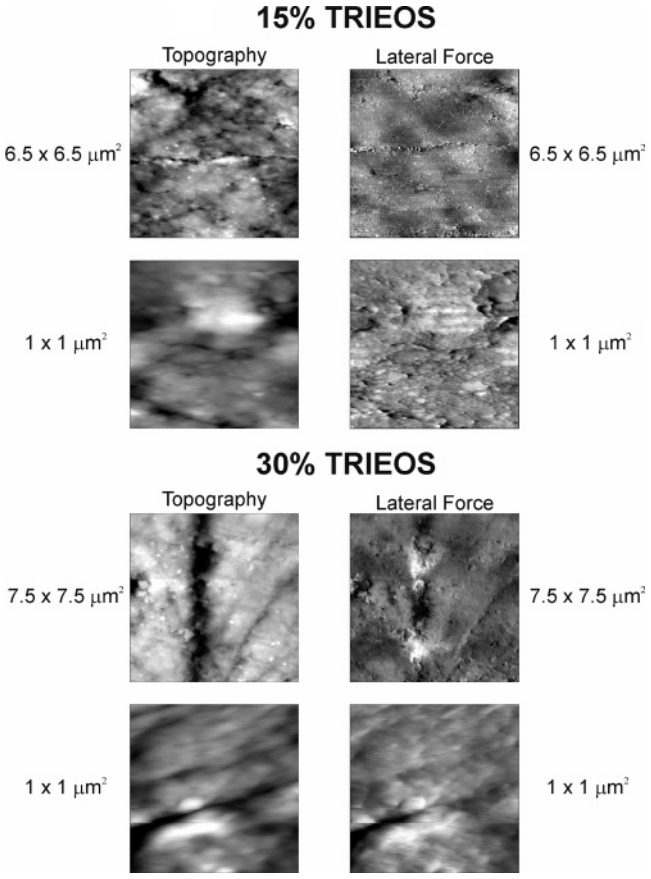


**Figure 5.** Topography (left) and lateral force (right) contact-mode AFM images of the polished surface on the nanocomposites based on HEMA containing 15 (top) and 30 (bottom) wt % proportion of TRIEOS.

Figure 6 shows the topographic and lateral force image of a $2 \times 2$ $\mu m^2$ area of a fresh fracture surface of the sample containing 15 wt % TRIEOS. Although fresh fracture surfaces are obviously much rougher than polished ones, in the submicrometer scale, the topography is very similar in both cases, as can be seen by comparing the topography image in Figure 6 and the $1 \times 1$ $\mu m^2$ topography image in Figure 5. Again, the lateral force image suggests a very homogeneous, smooth, random, uniform, and relatively featureless surface, without any clear indication of phase separation.

In summary, the AFM images presented in Figures 5 and 6 suggest that the hybrid materials are very uniform, with a homogeneous mixing of the inorganic and the organic components that could be depicted as a continuous phase corresponding to the polymer matrix, which "traps" the silica components at the molecular level via covalent bonding, with few or no silica islands, that in any case must be $<100$ nm, in agreement with the transparent appearance of the samples. This suggests that, in case segregated domains exist, they must be clearly smaller than the wavelength of visible radiation. This is understandable when taking into account the synthesis route selected to obtain these materials, which results in the silanol groups from the hydrolyzed inorganic silicates reacting rapidly with hydroxyl groups in the polymer chains to form covalent C−O−Si bonds, and was indeed to be expected, taking into account the results obtained by DSC (see below), according to which the polymer chains are confined in domains smaller than 15 nm, far below the resolution achieved in our AFM images.

Our AFM images can be compared with AFM images of similar resolution reported previously for similar hybrid materials with the same hybridation degrees,[25] where a clear correspondence between the transparency of the hybrid materials and the size of the segregated domains was also observed. The high homogeneity of these materials guarantees their optical properties and applications.

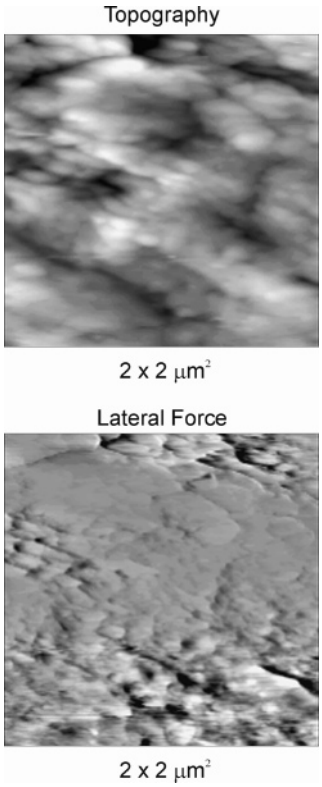


**Figure 6.** Topography (top) and lateral force (bottom) contact-mode AFM images of a $2 \times 2$ $\mu m^2$ area of the fresh fracture surface of the nanocomposite based on HEMA containing 15 wt % proportion of TRIEOS.

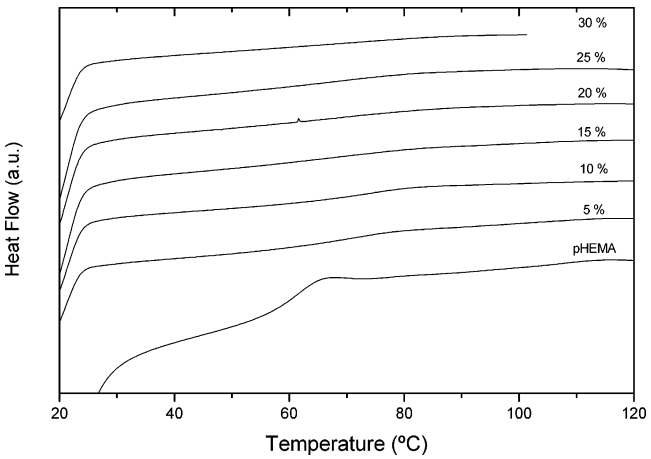


**Figure 7.** DSC thermogram of silica-containing hybrid materials based on HEMA with different wt % proportions of TRIEOS with the heating rate of 20 °C/min under nitrogen atmosphere.

**Thermal Stability.** The glass transition temperature ($T_g$) of hybrid materials based on PHEMA with increased weight proportion of TRIEOS up to 30% was analyzed by DSC, and the results are shown in Figure 7 and Table 2, together with those obtained with pure polymer PHEMA. The values obtained for the $T_g$ of these materials are lower than expected,[26] which could be related to the presence into the matrix of residual water, ethanol, and monomers acting as plasticizers. To confirm this hypothesis, some samples were subjected to a dried process under vacuum (≈8 h at 60 °C). After this treatment, the thermal

**TABLE 2: Thermal (Glass Transition Temperature $T_g$) Properties, Residual $SiO_2$ Content, Refractive Index ($n$), and Degree of Condensation of Hybrid Materials Based on HEMA with Increasing Weight Proportion of TRIEOS**

| material | $T_g$ (°C)[a] | $T_g$ (°C)[b] | residue at 800 °C in wt % | $n \pm$ 0.0005 | condensation degree (%) |
|---|---|---|---|---|---|
| 0% TRIEOS | 62 | 87 | 0 | | |
| 5% TRIEOS | 69 | 94 | 5.8 | 1.4995 | 94.0 |
| 10% TRIEOS | 74 | 99 | 10.4 | 1.4957 | 91.5 |
| 15% TRIEOS | 77 | | 16.4 | 1.4902 | 88.3 |
| 20% TRIEOS | | | 21.8 | 1.4857 | 87.4 |
| 25% TRIEOS | | | 26.4 | 1.4855 | 81.1 |
| 30% TRIEOS | | | 29.5 | 1.4800 | 77.7 |

[a] Experimental error = (±3 °C). [b] Glass transition temperature obtained after dried treatment of the samples.

stability of these materials increases significantly because the value of the $T_g$ increases in ≈25 °C (see Table 2).

As the silica content is increased, the $T_g$ peak becomes weaker and is shifted to a higher temperature. For a weight proportion of TRIEOS above 20%, well-defined $T_g$ cannot be observed. An absence of clear calorimetric glass transition has already been observed in other hybrid systems[27] and has been attributed to the confinement of polymer chains in domains smaller than 15 nm from which the characteristic long-distance motions of the glass transition phenomenon are restricted[28] due to both the cross-linking points generated from the formation of covalent bonding between the polymer chains and the silica network and the steric hindrance of the rigid silica framework. This result agrees well with the uniformity and fine morphology observed by AFM, appropriate for hybrid materials where the inorganic structure is homogeneously mixed at molecular scale with the organic component.

The thermal degradation process of hybrid matrixes based on PHEMA with increased wt % proportions of TRIEOS up to 30% was evaluated by thermogravimetry analysis (TGA) and derivate thermogravimetry data (DTG). It was found that these hybrid materials decomposed in different stages: The first one, which takes place at 50−200 °C, with a weight loss of about 5%, and is similar for all the selected matrixes, including the pure polymer PHEMA, basically came from residual solvents, water, and unreacted monomer. Then, a fast and continuous weight loss is observed in the 200−500 °C region, corresponding to the thermal depolymerization of polyacrylates, with a rate of decomposition depending on the environment of the polymer chains. At 800 °C, the solid residue of the samples is constituted by silica, and the residual weight in the TGA thermograms allows determination of the real inorganic contents in the hybrid materials. The experimental results reported in Table 2 are in good agreement with the theoretical weight proportion of TRIEOS selected to synthesize the parent hybrid materials.

**Infrared Spectroscopy.** The FT-IR spectra of the hybrid materials based on HEMA with different weight proportions of TRIEOS were recorded by using as baseline the infrared spectrum of the organic polymer, registered under otherwise identical experimental conditions, to avoid the overlap of PHEMA bending groups with bands of the inorganic phase in the nanocomposite spectra. The infrared spectra of all these materials have absorptions at 780, 920, and 1100 $cm^{-1}$ that are associated with the bending vibrations of Si−O−Si bonds, the stretching of Si−OH bonds, and the stretching vibration of Si−O−Si groups, respectively.[22] The intensity of these bands increases with increasing the TRIEOS content in the sample. Further structural information of these hybrid materials could be reached by $^{29}Si$ and $^{13}C$ NMR techniques, as described below.

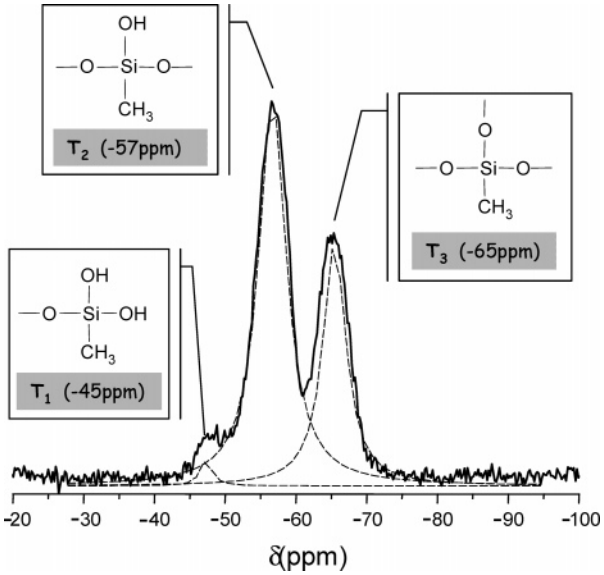


**Figure 8.** $^{29}Si$ CP-MAS high-power proton decoupling NMR spectrum corresponding to a sample of hybrid (HEMA 30 wt % TRIEOS). The spectrum was obtained with 6000 averages, a 5 s recycle delay, and a line broadening of 75 Hz. The resonances at −45, −57, and −65 ppm correspond to silicons with 1, 2, and 3 siloxane bonds to the silicon of interest.

**Solid-State NMR Spectroscopy.** The structure of the hybrid materials has been analyzed by NMR in solid state by trying to establish a direct relationship between the structure−microstructure of the hybrids and their laser behavior as a function of the proportion of inorganic component (TRIEOS) present in the material.

$^{29}Si$ NMR spectra can be expected to yield information related to both the chemical structure and the degree of condensation of the hybrids (HEMA 5−30 wt %TRIEOS). An example of a $^{29}Si$ NMR spectra of the hybrid (HEMA 30 wt %TRIEOS) is shown in Figure 8. Three signals at −45, −57, and −65 ppm were observed for each hybrid matrix assayed. The assignment of these peaks is based on previous studies on silica gel.[28,29] The peak at −45 ppm corresponds to the $T_1$ species and is attributed to the silicon atom bonded to two −OH groups and two order siloxane groups, represented by $CH_3SiO(OH)_2$. The peak $T_2$ at −57 ppm is related to the presence of a silanol group bonded to the inorganic structure of type $CH_3SiO_2OH$, and finally, the $T_3$ peak at −65 ppm is associated with silicon bonded to three siloxane groups, such as $CH_3SiO_3$.[30]

On the basis of the quantitative relationship of the signals, comparable under the same experimental conditions, it can be concluded from Figure 9 that these types of organic−inorganic hybrids exhibit a slow but progressive descent of the inorganic cross-linking degree as the proportion of TRIEOS into the material increases because a decrease of the $T_3$ groups is observed at the same time that the proportion of $T_2$ groups increases. The signal corresponding to the $T_1$ species, related to terminal groups, appears in matrixes with wt % proportions of TRIEOS higher than 20%.

By taking into account these structural results, a direct relationship could be established between the structure of the hybrid materials and their laser behavior: the chemical structure of the inorganic network dominated by di-/tri-substituted silicates, in a proportion ≈35:65, corresponding to samples of HEMA with 15 and 20 wt % proportion of TRIEOS, optimizes the lasing photostability of Rh6G. The density of the inorganic domains in the final material reached with this proportion of di-/tri-substituted silicates represent the best compromise be-

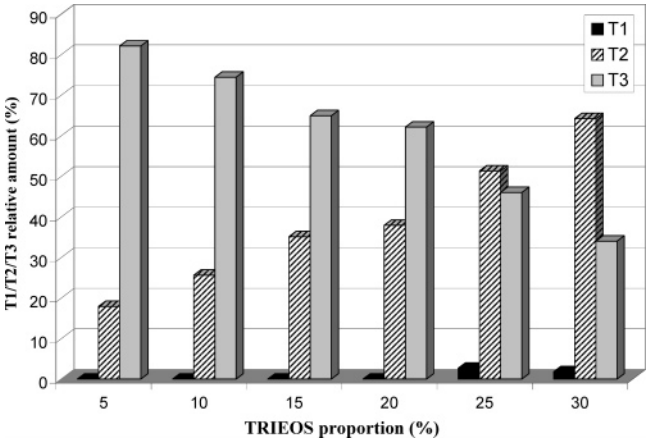


**Figure 9.** Quantitative relationship of the signals, comparable under the same experimental conditions, for the species $T_1$, $T_2$, and $T_3$ in the hybrid samples of (HEMA 5−30 wt % TRIEOS).

tween the enhancement of thermal dissipation of the matrix and the decrease of the photochemical degradation of the dye. Any variation in the proportion of these substituted silicates results in a drastic worsening of laser performance, reflecting, once again, that the rigidity of the inorganic network is of the uppermost importance in optimizing the laser action of a given dye.

No further peaks appeared in the CP/MAS-$^{29}$Si NMR spectra due to the presence of silicon bonded to an inorganic group in the different chemical environments studied. However, the chemical bond formation by the polycondensation between silica and hydroxyl groups of the organic monomer (HEMA) in these materials could be confirmed through CP/MAS-$^{13}$C NMR spectroscopy. The corresponding signal proves that a true bond exists between inorganic and organic domains, explaining the homogeneous optical and morphological properties of the so-obtained hybrid materials.

By keeping in mind the theoretical prediction of signs assignment of $^{13}$C, if there was polycondensation between the organic and the inorganic part, a new peak centered at 64.5 ppm has to be observed. As shown in Figure 10 in the HEMA/TRIEOS 25 wt % sample, a very small but defined peak is detected at 64 ppm, shielded by the other two big signals hindering its quantification. This signal was observed in all samples independent of its composition, while, in a HEMA/TEOS series previously studied, this peak was only detected for matrixes with a wt % proportion of TEOS higher than 15%.[17]

In addition, $^{29}$Si NMR spectroscopy was used to evaluate the degree of condensation (the relative number of siloxane bonds to each silicon atom) in the networks. Silicon atoms with different degrees of condensation existed in the TRIEOS system. Using the symbol $T_n$ to design the number of silicon atoms with $n$ siloxane bonds ($n = 0$, 1, 2, or 3), the degree of condensation was semiquantitatively determined, after the deconvolution of peaks, according to the equation:

$$\text{degree of condensation} = [1.0(\%\ \text{Area}\ T_1) + 2.0(\%\text{Area}\ T_2) + 3.0\ (\%\text{Area}\ T_3)]/3.0$$

Table 2 lists the degree of condensation of these hybrid materials, which decreases as the inorganic content of the matrix increases.

**Optical Properties.** The refractive index ($n$) measured for the hybrid materials, reported in Table 2 and shown in Figure 11, decreases linearly with increasing the silica content, with a behavior similar to that previously reported.[31] This result allows

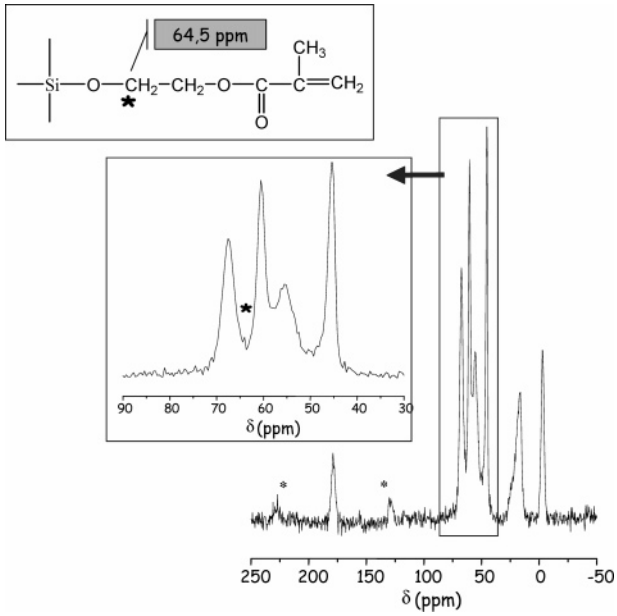


**Figure 10.** $^{13}$C CP-MAS high-power proton decoupling NMR specrtum corresponding to a sample of hybrid (HEMA 25 wt % TRIEOS). The spectrum was obtained with 800 averages, a 5 s recycle delay, and a line broadening of 5 Hz. The inset shows the vertical expansion of the spectrum between 30 and 90 ppm. The resonance observed at 64 ppm might be associated to the presence of chemical moiety produced by the chemical bonding between the organic and inorganic phases. The spinning sidebands corresponding to the peak associated with the carbonyl group are indicated with *.

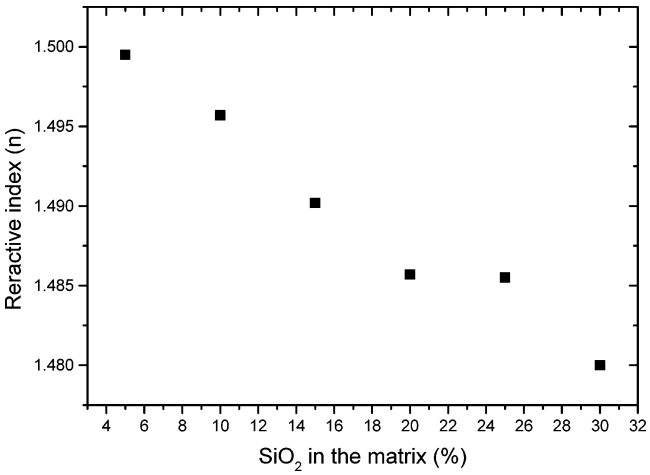


**Figure 11.** Dependence of the refractive index of the hybrid materials on the content of $SiO_2$ in the matrix.

the possibility of tuning the refraction index of these hybrid matrixes by modulating the silica content, which is of importance for the use of these materials in the field of micro- and nano-photonic devices (waveguides, emitting devices, and holographic materials).

Figure 12 shows the relationship between the refraction index and the condensation degree of the hybrid matrixes: the higher the refraction index, the higher the condensation degree, which is directly related to the density of the inorganic network.

## IV. Conclusions

In this paper, we report, for the first time to the best of our knowledge, a systematic study to relate the laser action from dyes doped into monolithic hybrid matrixes with the structural, morphological, optical, and thermal properties of the host

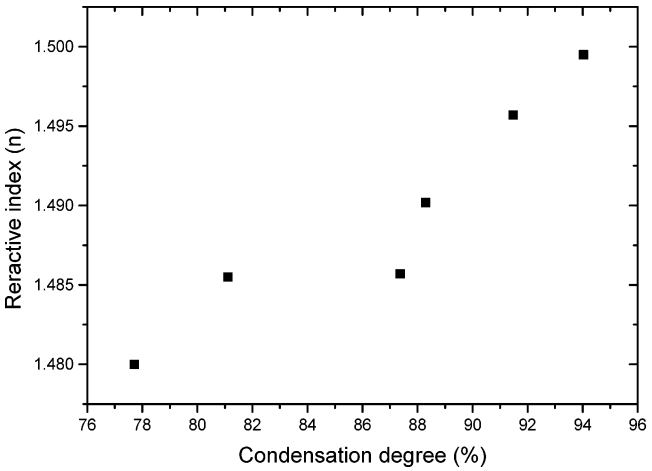


**Figure 12.** Variation of the refractive index of the hybrid materials with its degree of condensation.

material. Efficient and highly photostable laser operation was achieved from Rh6G and PM597 dyes incorporated into newly synthesized organic−inorganic hybrid materials based on HEMA or (HEMA/MMA 1:1 v/v) copolymer with TRIEOS as an inorganic phase added in weight proportions ranging from 5 to 30%. The laser action depended strongly on the composition of the matrix: For Rh6G, the highest photostability is achieved with the material (HEMA 20 wt % TRIEOS), where the laser output not only did not decrease but increased significantly with respect to its initial values, with the number of pump pulses in the same position of the sample at 10 Hz repetition rate and over a span of 100 000 pulses. PM597 resulted in being highly photostable, exhibiting a constant laser output without any sign of degradation after 100 000 pump pulses at 10 Hz, independent of the hybrid composition. When the pumping repetition rate was increased up to 30 Hz, increasing the weight proportion of TRIEOS resulted in higher photostability of PM597 due to the enhancement of the thermal dissipation provided by the silica content.

The structural analysis of these hybrid materials by solid-state NMR spectroscopy revealed that an inorganic network dominated by di-/tri-substituted silicates, in a proportion ≈35:65, corresponding to samples of HEMA with 15 and 20 wt % proportion of TRIEOS, optimizes the lasing photostability. Atomic force microscopic studies evidence a material with high homogeneity, with the silica particles uniformly dispersed in the polymer matrix in domains with sizes in the scale of nanometers. Miscibility between the silica and the monomer was enhanced by covalent bonding between the organic and inorganic components. The resulting structural and morphological uniformity led to the absence of a clear glass transition temperature. The prepared hybrid materials exhibited a refractive index that is tunable as a function of the silica content in the matrix, opening the way to their potential applications in optical devices.

All the obtained results demonstrate that the hybridation methodology followed in the present work allows synthesis of organic−inorganic materials without phase separation at the nanometric scale, combining the properties of inorganic glasses and organic polymers in an unique matrix.

**Acknowledgment.** This work was supported by projects MAT2000-1361-C04-01 and MAT2004-04643-C03-01 of the Spanish MCYT and project no. 7N/0100/02 of the Comunidad Autónoma de Madrid. O.G. thanks the MICYT for awarding her a Ramón y Cajal scientific contract. D.A. thanks the Comunidad Autónoma de Madrid for awarding him a predoctoral fellowship.

## References and Notes

(1) Nikogosian, D. N. In *Properties of Optical and Lasers Related Materials. A Handbook*; Wiley: New York, 1997; pp 388−391.
(2) Barnes, N. P. In *Tunable Lasers Handbook;* Duarte, F. J., Ed.; Academic Press: New York, 1995; pp 219−291.
(3) O'Connell, R. M.; Saito, T. T. *Opt. Eng*. **1983**, *22*, 393.
(4) Rahn, M. D.; King, T. A. *J. Mod. Opt*. **1998**, *45*, 1259.
(5) Costela, A.; García-Moreno, I.; Figuera, J. M.; Amat-Guerri, F.; Mallavia, R.; Santa-María, R. D.; Sastre, R. *J. Appl. Phys.* **1996**, *80*, 3167.
(6) Duarte, F. J. *Appl. Opt*. **1994**, *33*, 3857.
(7) Sastre, R.; Costela, A. *Adv. Mater*. **1995**, *7*, 198.
(8) Costela, A.; García-Moreno, I.; Sastre, R. In *Handbook of Advances Electronic and Photonic* Materials and Devices; Nalwa, H. S., Ed.; Academic Press: San Diego, CA, 2001; Vol. 7, pp 161−208.
(9) Faloss, M.; Canva, M.; Georges, P.; Brun, A.; Chaput, F.; Boilot, J. P. *Appl. Opt*. **1997**, *36*, 6760.
(10) Marlow, F.; McGehee, M. D.; Zhao, D.; Chmelka, B. F.; Stucky, G. D. *Adv. Mater*. **1999**, *11*, 632.
(11) Yariv, E.; Reisfeld, R.; Minti, H. *Opt. Mater*. **1999**, *13*, 49.
(12) Ahmad, M.; King, T. A.; Ko, D.; Cha, B. H.; Lee, J. *J. Phys. D: Appl. Phys*. **2002**, *35*, 1473.
(13) Duarte, F. J.; James, R. O. *Opt. Lett.* **2003,** *28*, 2088.
(14) Costela, A.; García-Moreno, I.; Gómez, C.; García, O.; Sastre, R. *Chem. Phys. Lett*. **2003**, *369*, 656.
(15) Yang, Y.; Wang, M.; Qian, G.; Wang, Z.; Fan, X. *Opt. Mater.* **2004**, *24*, 621.
(16) Costela, A.; García-Moreno, I.; Gómez, C.; García, O.; Sastre, R. *Appl. Phys. B* **2004**, *78*, 629.
(17) Costela, A.; García-Moreno, I.; Gómez, C.; García, O.; Garrido, L.; Sastre, R. *Chem. Phys. Lett.* **2004**, *387*, 496.
(18) Yang, Y.; Qian, G.; Wang, Z.; Wang, M. *Opt. Commun.* **2002**, *204*, 277.
(19) Sinha, S.; Sasikumar, S.; Ray, A. K.; Dasgupta, K. *Appl. Phys. B* **2004**, *78*, 401.
(20) Duarte, F. J. *Appl. Opt*. **1994**, *33*, 3857.
(21) Duarte, F. J.; Pope, E. J. A. *Ceram. Trans*. **1995**, *55*, 267.
(22) Hajji, P.; Davis, L.; Gerard, J. F.; Pascault, J. P.; Vigier, G. *J. Polym. Sci., Part B: Polym. Phys.* **1999**, *37*, 3172.
(23) Rodríguez, M.; Costela, A.; García-Moreno, I.; Florido, F.; Figuera, J. M.; Sastre, R. *Meas. Sci. Technol*. **1995**, *6*, 971.
(24) Nung, T. H.; Canva, M.; Dao, T. T. A.; Chaput, F.; Brun, A.; Hung, N. D.; Boilot, J. P. *Appl. Opt.* **2003**, *42*, 2213.
(25) Wei, Y.; Jin, D.; Brennan, D. J.; Rivera, D. M.; Zhuang, Q.; DiNardo, N. J.; Qiu, K. *Chem. Mater*. **1998**, *10*, 769.
(26) Wei, Y.; Jin, D.; Yang, C. H.; Kels, M. C.; Qiu, K.-Y. *Mater. Sci. Eng., C* **1998**, *6*, 91.
(27) Motomatsu, M.; Takahashi, T.; Nie, H.-Y.; Mizutani, W.; Tokumoto, H. *Polymer* **1997**, *38*, 177.
(28) Vaia, R. A.; Ishii, H.; Giannelis, E. P. *Chem. Mater*. **1993**, *5*, 1694.
(29) Chang, T. C.; Wang, Y. T.; Hong, Y. S.; Chin, Y. S. *J. Polym. Sci., Part B: Polym. Chem.* **2000**, *38*, 1972.
(30) Fonseca, M. G.; Oliveira, A. S.; Airoldi, C. *J. Colloid Interface Sci.* **2001**, *240*, 533.
(31) Yu, Y.-Y.; Chen, W.-Ch. *Mater. Chem. Phys*. **2003**, *82*, 388.